

# Thermal non-destructive characterization of rail networks by using Infrared Thermography and FEM simulation

Abdelhamid Noufid<sup>1,\*</sup>, Nadia Hidar<sup>2</sup>, Sougrati Belattar<sup>3</sup>, Mohamed Elafi<sup>4</sup>, and M'barek Feddaoui<sup>1</sup>

<sup>1</sup> LGEMS/Department of Mechanics and Civil Engineering, Ibn Zohr University, P.O. Box, Agadir, Morocco

<sup>2</sup> Cadi Ayyad University, Department of Chemistry, Marrakech, Morocco

<sup>3</sup> Physics Department, Semlalia, Faculty of Sciences, Cadi Ayyad University, Marrakech, Morocco

<sup>4</sup> Research Laboratory of Physics and Engineers Sciences, Sultan Moulay Slimane University, Beni Mellal, Morocco

**Abstract.** Because of the repeated passage of trains, anomalies are created inside the rails in the form of cracks of different shapes and position. These are due essentially to the wheel – rail contact. They present a hazard causing at the final stage rail failure, train derailment and accidents. Detecting track anomalies has become a major issue for the entire rail industry around the world. This paper focuses on the degradation of rails in urban railways in terms of cracks. The purpose is to develop an approach to detect and predict rail breaks, which will optimize maintenance task. Infrared thermography was used in order to characterise the effect of a defect on the acquired thermogram. Different defects were considered by varying their size, depth and inclination angle with respect to the rail surface.

## 1 Introduction

Infrared thermography is one of the effective Non-Destructive Testing (NDT) methods [1]. It could be used in the detection of internal defects [2]. This method which is based on thermal non-destructive control is rather simple to implement in practice. Several studies have been dedicated to its use in the detection of defects. They have shown its effectiveness in revealing the presence of defects in inspected parts [3-8].

In this work, we are interested in the detection of internal cracks located in rails by means of infrared thermography. After subjecting the surface of the structure to a natural heat flux excitation, the temperature contrast obtained at the surface can be indicative of the presence of a possible internal defect. But, how detectability can be feasible? The purpose of this study is to investigate the influence of the size and the position of an internal defect of crack type on the thermal response of the studied structure surface. The methodology used is based on the finite elements modelling of the heat transfer problem taking place in the rail structure. Simulations of different conditions of the defect configuration are performed. The corresponding thermal images are investigated. It was found that these are similar to those provided by real infrared cameras. This holds however only if the conditions regarding the achieved contrast remain within the sensitivity range of the cameras used [9]. One of the pursued objectives is to determine at which depth and with which inclination of a crack defect, detection is possible.

## 2 Materials and methods

Infrared thermography approach is used here to show up the presence of internal defects in rails. The ability of this method to detect a crack defect in the rail structure is considered under the following conditions. After subjecting the rail surface to a heat flux excitation, the contrast of the obtained stationary temperature at the surface of the rail is analysed. This provides information that can be employed to come to a decision regarding the eventual presence of a defect.

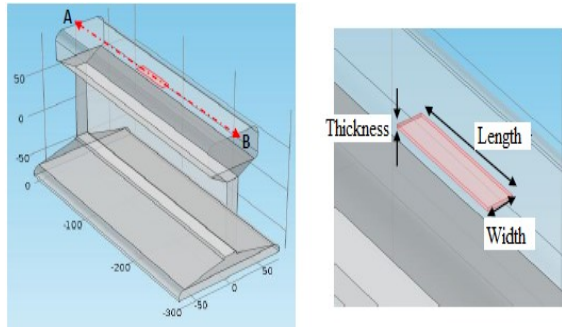
Considering different scenarios of defects in a rail, the finite elements methods is used by means of a commercial software in order to get through simulation the associate thermographic images. These thermograms of the rail surface vary depending on the actual thermo-physical properties of the rail. They are like this sensitive to the defect extent and its distance from the rail surface. Evolution of thermograms can be monitored to reveal the existence of some defect in the inspected zone of the rail.

Fig. 1 presents the geometry of the rail structure that was used for finite elements simulations. The figure indicates also the characteristics of an internal defect present in the rail structure. The defect is modelled under the form of a parallelepiped air volume having the following dimensions: length  $L = 50mm$ , width  $l = 10mm$  and thickness  $e = 1mm$ .

Simulations were performed under stationary regime. The prescribed boundary conditions are shown in Fig. 2. They correspond to the following: the rail top surface is subjected to a heat flow  $\varphi = 24kW/m^2$ , the bottom

\* Corresponding author: [a.noufid@uiz.ac.ma](mailto:a.noufid@uiz.ac.ma)

surface of the rail is maintained at the constant ambient temperature  $T_a = 25^\circ\text{C}$ , and the lateral sections surfaces of the rail are assumed to be isolated with zero heat flux crossing them  $\varphi = 0$ .



**Fig. 1.** Geometry of the considered rail structure and defect.

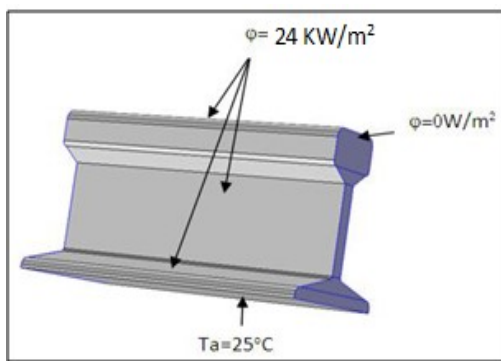


**Fig. 2.** Boundary conditions of the rail structure domain model.

With these hypotheses, simulations are conducted in order to study the effect of key parameters on the thermal images. These include the depth of the defect with respect to the upper surface of the rail and the orientation of the plane of this defect by reference to horizontal plane parallel to the upper surface of the rail. Temperature is extracted for all points belong to an axis denoted [AB] which is located on the upper surface of the rail (centred and parallel to the longitudinal rail direction, see Fig. 1). The rail material is assumed to be made of steel, while the defect domain is modelled as air. The associated thermal characteristics are shown in Table 1.

**Table 1.** Thermal characteristics of the materials used.

Materials	Thermal conductivity (W/m.K)	Heat capacity (J/kg.K)	Density ( $\text{kg/m}^3$ )
Steel	45	473	7801
Air	0.025	1012	1.164

### 3 Results and discussion

#### 3.1 Influence of defect depth

In this section, the influence of the defect depth on its appearance on the synthesized thermal images is studied. For this purpose, the dimensions of a horizontally oriented defect were fixed at  $50 \times 10 \times 1 \text{ mm}$ , and its depth was varied in the following set:  $p = 0.1, 0.2, 0.5, 1, 2, 5 \text{ mm}$ . The obtained results in terms of upper rail surface thermograms are shown in Fig. 3.

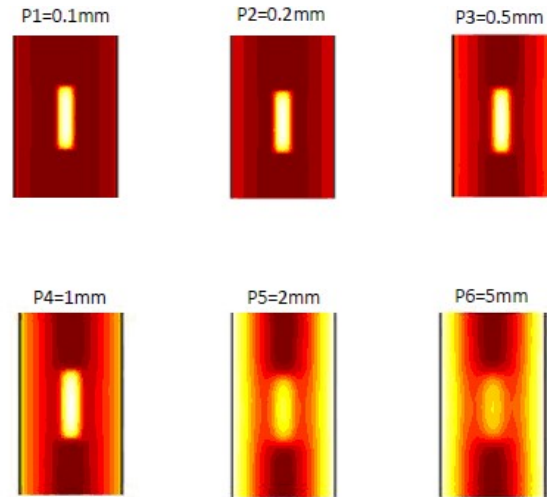


**Fig. 3.** Thermal images for different depths of defect.

Fig. 4 presents the various profiles as obtained for the six considered cases along the segment [AB]. From this figure, it is clear that the contrast is more obvious when the defect depth approaches the rail surface. This shows that the closer the defect moves towards the upper surface, the more easier becomes its detection based on the contrast observed on temperature profile  $\Delta T$ .

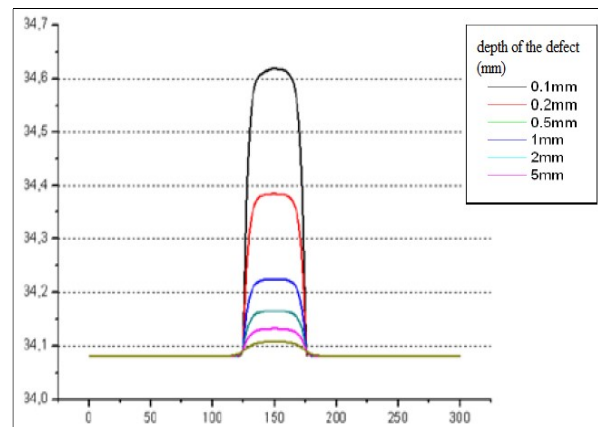


**Fig. 4.** Temperature distribution along the AB axis

An infrared camera detects the temperature difference  $\Delta T$ . This difference in temperature was materialized here as a contrast observed on the obtained thermogram. For a high sensitivity camera, even a smaller  $\Delta T$  can be detected, and referring to the actual analyzed cases, even deep cracks could be distinguished. To highlight this fact, Table 2 presents the calculated difference in temperature for the six studied depths.

**Table 2.** Temperature difference as function of defect depth.

Depth (mm)	0.1	0.2	0.5	1	2	5
Temperature difference (°C)	0.54	0.30	0.14	0.07	0.06	0.03

### 3.2 Influence of defect orientation

In this section, the influence of the defect plane orientation on the related thermal image is studied. The dimensions of the defect are chosen to be  $50 \times 10 \times 1 \text{ mm}$ . Fig. 5 shows the orientation of the defect plane as determined by the orientation angle which is measured from the horizontal plane. The depth of the horizontal plane was fixed at  $0.2 \text{ mm}$  and the defect orientation angle was varied according to the following sequence:  $0^\circ$ ,  $15^\circ$ ,  $30^\circ$ ,  $45^\circ$ ,  $60^\circ$  and  $75^\circ$ .

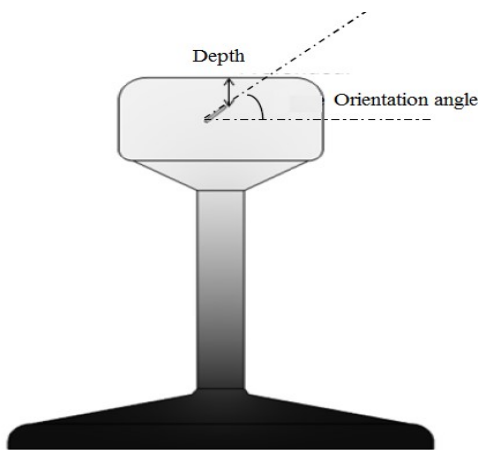


**Fig. 5.** Schematization of defect orientation

Fig. 6 presents the obtained thermograms as function of the orientation angle.

Fig. 7 presents the obtained traces for the six considered cases of defect orientation along the segment  $[AB]$ .

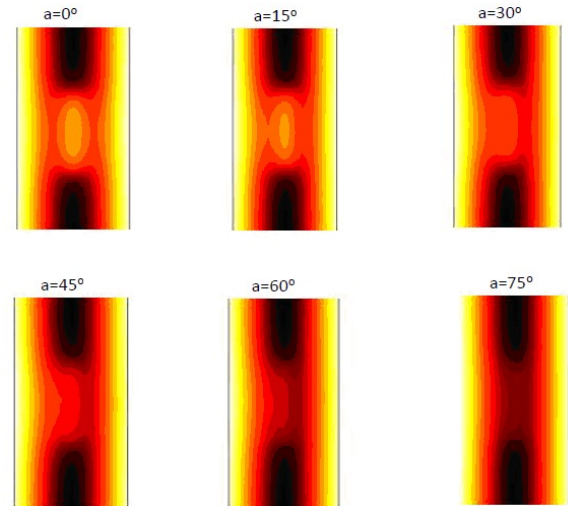
Table 3 summarises the difference in temperature as function of the considered orientation angle.

**Table 3.** Temperature difference for different orientation angles of defect.

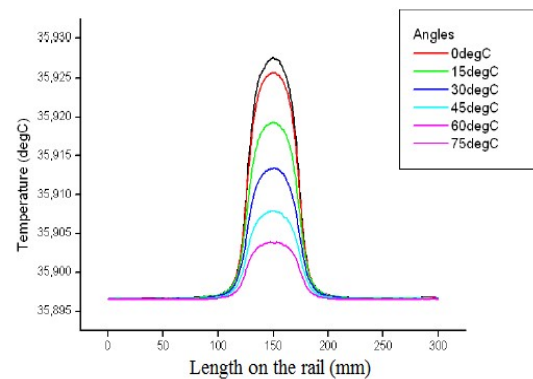
Angle (°)	0	15	30	45	60	75
Temperature difference (°C)	0.31	0.29	0.23	0.17	0.11	0.07

Fig. 6 shows that the defects traces in the obtained thermograms tend to disappear when the orientation angle of defect plane increases. However, one can see that the profile along the segment  $[AB]$  remains theoretically visible, but the contrast is very small for high orientation angles. This is corroborated by the amplitudes of traces curves as given in Fig. 7. One can see that the detection of a horizontal defect (angle  $0^\circ$ ) is easier than for higher orientation angles. In the case for which this angle is equal to  $75^\circ$ , the contrast is too small

yielding to difficulties in catching the signature at a practical level. High resolution cameras are needed in this last case, but noise may also impede performing detection and the defect may remain quite invisible. As seen in Table 3, the defect corresponding to the orientation angle  $75^\circ$  shows only a temperature variation which intensity is equal to  $0.07^\circ\text{C}$ . So, the defect may be undetectable with an ordinary infrared camera.



**Fig. 6.** Thermal images as function of the orientation angle of defect plane.



**Fig. 7.** Thermal images profiles along the segment  $[AB]$  for different defect orientation angles

## 4 Conclusions

This study was dedicated to crack detection in a rail by means of infrared thermography method. Simulations based on the finite elements methods were performed to analyse the effects of several parameters. As a general defect can be horizontal or oblique, deep or superficial, the simulations were realized in order to assess the influence of the depth and the defect orientation on the contrast of thermal images.

The results have shown that, for a horizontal defect, the depth is an essential element in detection. A defect which is closer to the rail surface is easier to detect with an infrared camera. A defect located at a depth of  $5 \text{ mm}$  requires that sensitivity of the camera should be less than  $\Delta T = 0.3^\circ\text{C}$ .

For an oblique effect, the orientation plays a determining role in the detection of the defect. It has been shown that a horizontal defect is easier to detect, whereas a defect oriented by angle  $75^\circ$  from the horizontal is complicated to detect. This defect requires an infrared camera with a sensitivity of less than  $\Delta T = 0.07^\circ\text{C}$ , which is quite difficult within the framework of the current technologies.

## Acknowledgements

This article and the research behind it would not have been possible without the exceptional support of Miss Amal Satif. Her enthusiasm, knowledge and attention to detail have been a source of inspiration and have kept our work on track from the first draft to the final version of this document.

## References

1. C. Luigi, E. Rizzo. *J. Cons. Bui. Mat.* **154**,1139-1150 (2017)
2. S. Belattar, J. Rhazi, A. Elballouti. *Int. J.Mic. Mat. Pro.* **7**, 235-253 (2012)
3. A. Noufid, S. Belattar. *Iranian J. Sc. Tech. Tran. C. Eng.* **45**:187–196 (2021)
4. A. Noufid, S. Belattar. *J. Eng. R.* **9** (1), 86-104 (2021)
5. A. Eddazi, S. Belattar. *J. Eng. Tec.* **6**, 375-384. (2017)
6. A. Eddazi, S. Belattar. *J. Eng. Tec.* **6**, 215-219 (2017)
7. M. Elafi S. Belattar, R. Bouferra. *J. Eng. Tec.* **6**, 449-461 (2017)
8. M. Elafi, S. Belattar. *J. Eng Tec*, **6**, 329-339 (2018)
9. B. I, Shagdyrov, A. O. Chulkov, V. P. Vavilov, V. O. Kaledin & M. Omar. *Russ. J. N. T.*, **56**, 1083-1090 (2020)